Journal of Magnetic Resonance 204 (2010) 256–265

Contents lists available at ScienceDirect

Journal of Magnetic Resonance

journal homepage: www.elsevier.com/locate/jmr

On the practical aspects of recording wideline QCPMG NMR spectra

Ivan Hung, Zhehong Gan *

Center of Interdisciplinary Magnetic Resonance, National High Magnetic Field Laboratory, 1800 East Paul Dirac Drive, Tallahassee, FL 32310, USA

ARTICLE INFO

Article history:
Received 19 January 2010
Revised 2 March 2010
Available online 6 March 2010

Keywords:
NMR
CPMG
QCPMG
WURST
Second-order phase
^{35}Cl
Solid-state
NHMFL
Zirconocene dichloride

ABSTRACT

The practical aspects of applying CPMG for acquisition of wideline powder patterns are examined. It is shown that most distortions/modulations of spikelet spectra can be traced to the incoherent signal averaging from multiple coherence transfer pathways. A strategy for minimizing these distortions/modulations is described. Also, a few interesting observations regarding the implementation of the wideline WURST-QCPMG experiment are presented, namely the accumulation of second-order signal phase and the effects of varying the sweep rate and rf field of chirp pulses.

1. Introduction

There is much interest in the investigation of quadrupolar nuclei in non-spherically symmetric chemical sites which give rise to NMR patterns spanning hundreds to thousands of kHz, so called 'wideline' spectra. This interest stems largely from the ubiquity of quadrupolar nuclei, which represent ~75% of the NMR-active nuclei in the Periodic Table and thus constitute integral components of many industrially and biologically relevant substances [1–13]. Many quadrupolar nuclei (nuclei with spin quantum numbers greater than 1/2) exhibit poor sensitivity due to low gyromagnetic ratios, low natural abundances and/or strong interaction between their electric quadrupole moments with surrounding electric field gradients.

The quadrupolar Carr–Purcell Meiboom–Gill (QCPMG) experiment [14] is a method for signal enhancement of quadrupolar nuclei adapted from the CPMG sequence [15,16]. Using the QCPMG sequence, the magnetization is refocused repetitively giving rise to a train of echoes, which upon Fourier transformation gives a set of spikelets with a manifold resembling the conventional powder pattern. Since all the intensity is allocated into sharp spikelets, a large gain in signal-to-noise ratio (S/N) is obtained at the expense of resolution, which is dictated by the spikelet separation. The (Q)CPMG pulse sequence has been applied on numerous occasions to facilitate the acquisition of dilute or unreceptive quadrupolar nuclei including ^{2}H [17], ^{14}N [18,19], ^{17}O [20,21], ^{25}Mg [9,22–25], ^{27}Al [26–28], ^{33}S [29], ^{35}Cl [13,30–32], ^{39}K [24,33,34], $^{47/49}$Ti [35–37], ^{53}Cr [11], ^{55}Mn [38], ^{59}Co [39], $^{63/65}$Cu [7], ^{67}Zn [8,24,40–47], ^{87}Rb [48], ^{87}Sr [24], ^{91}Zr [23,49], ^{93}Nb [50], ^{95}Mo [51,52], $^{135/137}$Ba [53] and ^{209}Bi [54], as well as some spin-1/2 nuclei [21,55–64]. It is interesting to note that the CPMG sequence had been used since early on for sensitivity enhancement of spin-1/2 nuclei, such as ^{13}C [58,59,65] and ^{89}Y [60], as well as for discerning homogeneous and inhomogeneous contributions to solid-state line widths [65–67]. CPMG acquisition has also proven beneficial in combination with magic angle spinning (MAS) [68,69] and two-dimensional experiments, such as magic-angle-turning [70] and multiple-quantum correlation techniques [20,26,27,71–74]. In addition, it has recently been shown that the rapid cyclical refocusing of QCPMG makes it an ideal experiment for application in powered resistive magnets due to its reduced sensitivity to field inhomogeneity and instability [75].

The typical excitation bandwidth of monochromatic radio frequency (rf) pulses is limited to a range of ~200 kHz by currently achievable rf amplitudes and the Q factor of NMR probes. Therefore, for patterns with breadths greater than the excitation bandwidth, the full spectrum must be reconstructed from segments acquired at different offset frequencies [4,5,28,49,76–78]. Attempts at overcoming excitation bandwidth limitations for quadrupolar nuclei have recently been reported which include the use of microcoils [79–81] or frequency-swept pulses [81–84]. In particular, the combination of either of these techniques with QCPMG has much potential [81].

* Corresponding author. Fax: +1 850 644 1366.
E-mail address: gan@magnet.fsu.edu (Z. Gan).

1090-7807/$ - see front matter © 2010 Elsevier Inc. All rights reserved.
doi:10.1016/j.jmr.2010.03.001

In this work, several aspects concerning the acquisition of wideline spectra using the QCPMG and WURST-QCPMG experiments are examined. In particular, the effects of varying the pulse sequence parameters on the resulting time-domain signal and frequency-domain spectra are investigated. It is shown that many spectral distortions can be caused by destructive interference between the two coherence transfer pathways (denoted $p = +1$ and -1) selected by a two-step CPMG phase cycling scheme. Therefore, pulse sequence parameters should be set appropriately to ensure that the two pathways always average coherently. In cases where this might not be possible, the two coherence pathways can be separately recorded and processed prior to being combined; noting that this requires a doubling of the number of acquired transients and a consequent loss in efficiency by a factor of $\sqrt{2}$. Considerations regarding: (a) the enhancement in S/N, (b) optimal processing methods and (c) simulation of QCPMG spectra (including the effects of dynamics) have been reported in the literature [27,68–70,85–87] and will not be discussed.

2. Experimental

The sample of zirconocene dichloride Cp_2ZrCl_2 was purchased from Strem Chemicals, Inc. and used without further purification. A 19.6 T (830 MHz) narrow bore magnet equipped with a Bruker DRX console was used to acquire spectra at the Larmor frequency of ^{35}Cl (81.6 MHz). A single-resonance home-built probe using a 4.0 mm Samoson MAS stator was used for all experiments. Parafilm plugs were used to restrict the sample volume to the middle 5 mm of the rotor to coincide with the coil position, as well as to minimize exposure to air and moisture. The ^{35}Cl anisotropic NMR parameters of Cp_2ZrCl_2 have been reported previously [13]. All spectra were externally referenced by setting the ^{35}Cl resonance of a saturated NaCl(aq) solution to $\delta_{iso} = 0.0$ ppm.

2.1. The CPMG pulse sequence

The 'Carr–Purcell Meiboom–Gill' (CPMG) experiment [15,16] is used extensively for the measurement of T_2 transverse relaxation constants and consists of an excitation unit followed by a cycle (henceforth denoted as a CPMG cycle) containing a refocusing and an acquisition unit, which is repeated M times (Fig. 1a). The excitation unit is usually a simple monochromatic pulse with a flip angle of 90° followed by a τ_1 delay, which is used to position the resulting echo maxima in the middle of the τ_a acquisition periods. A 180°-pulse is often employed within the refocusing unit to maximize the refocusable signal. This pulse is sandwiched by a pair of τ_2 delays which reduces artifacts from probe ringing. The length of the acquisition period (τ_a) dictates the separation of spikelets ($1/\tau_a$) in the frequency-domain after Fourier transformation of the time-domain signal. Notably, the definition of τ_1 should take into account the finite length of p1 such that $\tau_1 = (\tau_a - p1)/2$. The power of the CPMG experiment stems from the simplicity of its pulse sequence, which requires little (if any) optimization of parameters:

1. p1 and p1 are set to maximize the signal (usually by using $\pi/2$ and π-pulses),
2. τ_1 is set to $(\tau_a - p1)/2$,
3. τ_2 is set to reduce the effects of probe ringing,
4. τ_a is set to capture most (or all) of the full-echo, and
5. M is set to acquire as many echoes as possible/necessary.

For MAS spectra, the entire CPMG cycle should be synchronized to the rotation period $\tau_r = 1/\nu_r$, such that $2N\cdot\tau_r = 2\tau_2 + p2 + \tau_a$, where N is an integer [68].

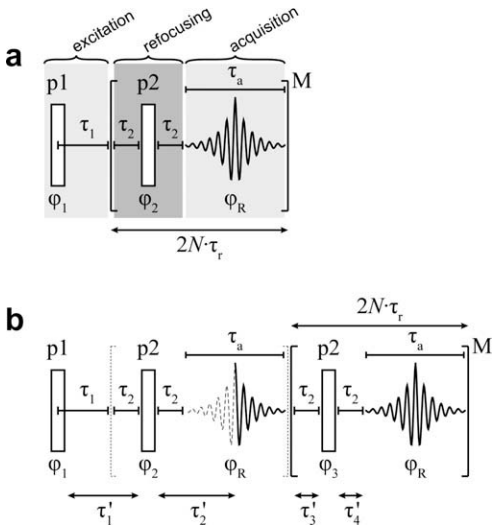

Fig. 1. (a). Schematic of the CPMG pulse sequence. (b) Schematic of the conventional (Q)CPMG implementation used for acquisition of quadrupolar powder patterns from Ref. [14]. The phase cycling scheme for (a) is $\varphi_1 = \varphi_R = \{0, \pi\}$ and $\varphi_2 = \pi/2$, while the phase cycling of (b) can be found in Ref. [14]. Parameters: p1 and p2 are the excitation and refocusing pulses, τ_a is the acquisition time for each echo which determines the spikelet separation $1/\tau_a$ after Fourier transformation. The τ_1 delay should be set equal to $(\tau_a - p1)/2$, while the τ_2 delays should be set appropriately to reduce the effects of probe ringing. The $\tau_{n'}$ delays commonly defined for the conventional (Q)CPMG experiment can be related to τ_1 and τ_2 as shown in (b). For the case of MAS, the CPMG cycle should be synchronized with the rotation period (τ_r) to ensure proper echo formation.

The CPMG phase cycling scheme contains a total of two steps: (0, π) alternation of the p1 and receiver phases (φ_1 and φ_R), and a fixed p2 phase (φ_2) which is offset by 90° from φ_1. The two-step φ_1 phase cycle ensures that only the $p = \pm 1$ single-quantum (1Q) coherences are retained for the p1 pulse, while a fixed φ_2 pulse phase means that all coherence orders (i.e., $p = \{+1, 0, -1\}$) generated by p2 are allowed to contribute to the signal. It has been shown that a considerable portion of the signal may pass through zero-quantum (0Q) coherence order when spectra exhibit significant frequency offsets, or p2 is not a pure π-pulse (i.e., the flip angle is not exactly 180°) [88–90]. Simulations illustrating this are shown in Fig. 2. A typical CPMG free-induction decay (fid) is shown in Fig. 2a, which was simulated by filtering the signal to keep only the $p = \pm 1$ coherences right after p1, in line with the experimental pulse sequence. The signal resulting from filtration of the signal after *every* p2 pulse keeping only the $p = \pm 1$ coherences is shown in Fig. 2b. The fid consists of only Hahn echoes, i.e., echoes from evolution of the magnetization solely in the transverse plane. Note that the first echo remains completely unperturbed, while a significant loss of intensity is observed for subsequent echoes. Thus, the first echo is a pure Hahn echo, while subsequent echoes are a combination of Hahn and stimulated echoes [91], i.e., echoes which form due to coherence transfer pathways that pass through 0Q order. The amount of observable signal is therefore maximized by the use of a minimal phase cycling scheme.

In addition to the simplicity of the pulse sequence and the minimal phase cycling scheme, the symmetry of the repetitive cycle also makes the CPMG pulse sequence an extremely robust experiment. The timings within the pulse sequence are such that all possible coherence transfer pathways (i.e., any combinations of $p = +1$, 0, −1 evolution periods) eventually form echoes at the same point in time (in the middle of the τ_a periods). This remarkable condition ensures that all coherence pathways taken by the magnetization always combine additively. Instances where different coherence transfer pathways interfere destructively will be discussed further below.

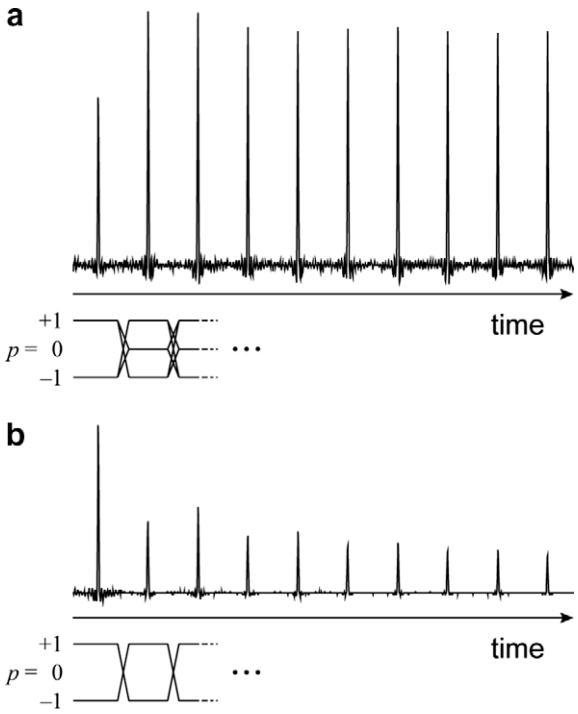

Fig. 2. Simulated ^{35}Cl QCPMG NMR signal of Cp_2ZrCl_2 (a) without coherence filtration after p2 pulses and (b) with filtration of the $p = 0$ coherence after every p2 pulse, i.e., keeping only the $p = \pm 1$ coherences. Time-domain signals are shown using the same vertical scale. Coherence transfer pathways are shown below the fids for illustration. Simulations were performed using SIMPSON [92] and the experimental parameters described in the caption of Fig. 4.

2.2. The conventional QCPMG pulse sequence

To our knowledge, usage of the CPMG experiment for signal enhancement of spin-1/2 NMR spectra was first reported in the late 1980s [58,60]. It was not until the late 1990s that this experiment was used for signal enhancement of quadrupolar nuclei ($I > 1/2$) [14]. The experiment has since been prefixed with the letter 'Q' to denote this particular application as the 'quadrupolar' Carr–Purcell Meiboom–Gill (QCPMG) sequence. However, it should be noted that there is *no fundamental difference* between the CPMG and QCPMG experiments. The two different names given to the same experiment only serve to differentiate between its applications to spin-1/2 or quadrupolar nuclei. With the new application of CPMG to quadrupolar nuclei also came a major shift towards the presentation of powder patterns as spikelet spectra, which results from Fourier transformation (FT) of the echo train, rather than FT after summation of the CPMG echoes. It has been shown using simulations and experiments that the envelope of the spikelet manifold resembles the appearance of conventional powder patterns [14].

A schematic of the conventional (Q)CPMG experiment [14] is shown in Fig. 1b. This sequence contrasts with the previously presented CPMG sequence (Fig. 1a) in three aspects. Firstly, one of the CPMG cycles is taken out of the M loop and the first half-echo is discarded. Secondly, instead of two inter-pulse delays (τ_1 and τ_2), four τ'_n delays are defined (these can be related to τ_1 and τ_2 as shown in Fig. 1b). Thirdly, a longer phase cycling scheme of 16 steps is employed compared to the two-step phase cycle shown earlier.

To our knowledge, the sole purpose for discarding the first half-echo of the fid is so that the resulting spikelet spectrum may be phased absorptively without the need for a large first-order phase correction. However, discarding the initial half-echo contradicts the purpose of signal enhancement and causes baseline distortions if spectra are presented in absolute value/magnitude mode (as many researchers are in the habit of doing). Hence, acquisition of the fid beginning from the first full-echo as in Fig. 1a is recommended. With full-echo acquisition, signal is not discarded and frequency-domain spectra may be presented as: (1) magnitude spectra with minimal baseline distortion, or (2) absorptively-phased spectra using a predictable amount of first-order phase correction (*vide infra*).

The inter-pulse delays in the (Q)CPMG sequence $\tau'_1, \tau'_2, \tau'_3, \tau'_4$ are related to the delays in the CPMG experiment (τ_1, τ_2) as shown in Fig. 1b. Care must be taken to set the τ'_n inter-pulse delays appropriately (as outlined in Section 2.1) to minimize distortions of the spectrum. Many literature examples have been found where the delays have been set such that $\tau'_1 = \tau'_2 \sim \tau'_3 = \tau'_4$ without regard for the length of τ_a. When the inter-pulse delays are set in such a manner, (Q)CPMG spectra will exhibit distortions that are sensitive to the p2 flip angle if a two-step phase cycle is employed (Fig. 3a). Modulation of the spikelet manifold arises due to the difference in time at which Hahn and stimulated echoes form, as has been previously reported [55,93]. The stimulated echoes which interfere destructively arise primarily due to the 0Q coherence created by the first p2 pulse (Fig. 3b, red dashed lines). Hence, the severity of the spectral distortion is correlated to an increase in the magnitude of the 0Q coherence as the flip angle of p2 deviates from 180°. For this reason, the conventional QCPMG pulse sequence [14] employs a 16-step phase cycle to filter out this 0Q contribution to the fid. Due to the symmetry of the CPMG cycle, 0Q coherences created within the cycle only contribute constructively to the signal. In any case, the appropriate settings for the τ'_n delays in Fig. 1b should be $\tau'_1 = \tau'_2 = \tau'_a/2 + \tau'_3$ and $\tau'_3 = \tau'_4$.

It is reiterated here that *there is no fundamental difference* between the two CPMG implementations in Fig. 1. As long as the inter-pulse delays for the (Q)CPMG sequence in Fig. 1b are set appropriately according to the guidelines in Section 2.1, the spectral distortion mentioned above will be avoided regardless of the p2 flip angle. However, for the sake of simplicity and maximum signal, the authors recommend using the CPMG sequence in Fig. 1a, which *will be the basis for all discussion henceforth*.

2.3. First-order phasing and the interference of multiple coherence transfer pathways

First-order phasing is defined so that a shift of the time-domain signal by a single dwell interval is equivalent to a phase difference of 360° in the frequency-domain spectrum. The first-order phase correction is defined as:

$$ph_1(\tau_e) = S \cdot \exp(i2\pi \cdot \frac{\tau_e}{dw} \cdot \frac{f}{sw}) = S \cdot \exp(i2\pi \cdot \tau_e \cdot f) \quad (1)$$

where S is the frequency-domain signal, τ_e is the position of the echo maximum in the time-domain, dw is the dwell time between adjacent real data points, sw is the spectrum width and f is the frequency variable ranging from $-sw/2$ to $+sw/2$. Spikelet and full-echo spectra (i.e., spectra for which the echo maximum is not at the start of the fid) may be phased straightforwardly by using a first-order phase approximately equal to $360° \cdot \tau_e/dw$. For CPMG spectra acquired using the sequence in Fig. 1a, the first-order phase correction would be $\approx 360° \cdot \tau_a/(2\,dw)$. A distortionless baseline may at times be difficult to obtain for phased spectra due to overlap between the spikelets. In such instances, presentation of CPMG spectra in the conventional powder pattern form (by summation of the time-domain echoes prior to FT) rather than spikelets is advisable (e.g., Fig. 8 of Ref. [27]).

Many researchers choose to present CPMG spectra in absolute value/magnitude mode. Although such presentation proves conve-

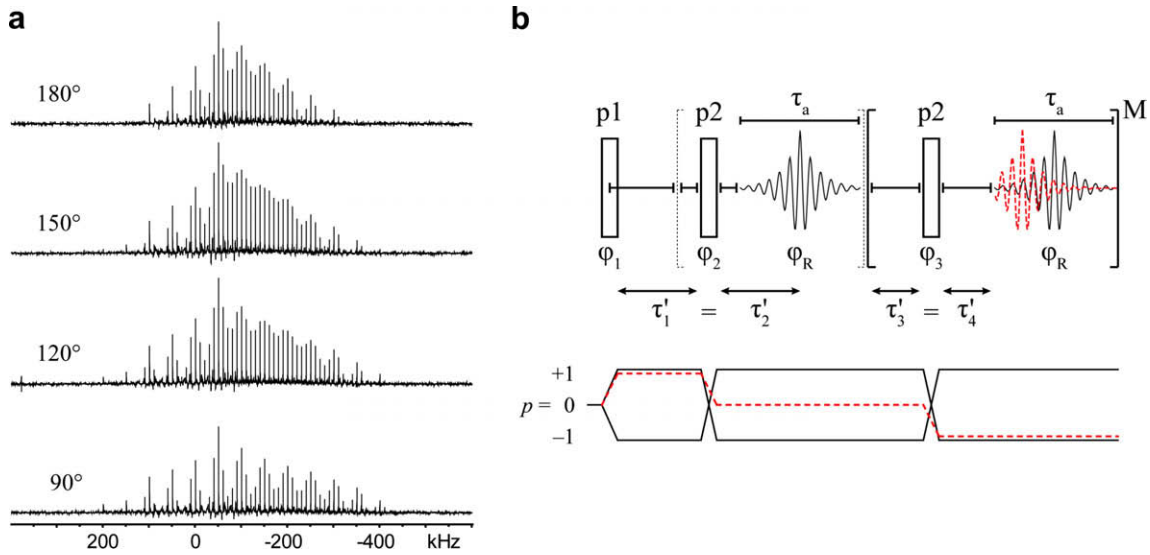

Fig. 3. (a). Modulations of the ^{35}Cl QCPMG NMR spikelet spectra of Cp_2ZrCl_2 at 19.6 T varying the 'selective' flip angle of p2 (shown on left) using rf fields of 90.9 kHz and the pulse sequence in Fig. 1b with p1 = 1.35 μs, $\tau'_1 = \tau'_2 = 50$ μs, $\tau'_3 = \tau'_4 = 20$ μs, τ_a = 100 μs, M = 40, *sw* = 1.0 MHz, a recycle delay of 1.0 s and a two-step phase cycle: $\varphi_1 = \varphi_R = \{0, \pi\}$ and $\varphi_2 = \varphi_3 = \pi/2$. Central-transition 'selective' pulses have durations reduced by the factor $(I + 1/2)$; for the case of ^{35}Cl ($I = 3/2$), conventional pulse widths are divided by 2. (b) Schematic of the conventional QCPMG pulse sequence illustrating the contribution of a stimulated echo (dashed red line) to the nominal QCPMG signal (solid black line) when using a two-step phase cycling scheme: $\varphi_1 = \varphi_R = \{0, \pi\}$ and $\varphi_2 = \varphi_3 = \pi/2$. Shown below the pulse sequence is the coherence transfer pathways for the stimulated echo (dashed red line) and nominal Hahn echoes (solid black lines). (For interpretation of color mentioned in this figure the reader is referred to the web version of the article.)

nient and baseline imperfections can be concealed, the authors advise against it because a crucial feature of white-noise is lost: the ability to *correctly* estimate *S*/*N* from the ratio between peak height and the noise level in a region without resonances. Absolute value spectra have reduced root-mean-square noise leading to an artificial increase in the *S*/*N*. Furthermore, the magnitude calculation is an irreversible process which discards part of the information content available and complicates least-squares fitting of spectra due to the uneven distribution of the noise power density. Thus, the use of absorptively-phased spectra (whenever possible) is recommended, particularly for spectral fitting and the measurement and comparison of *S*/*N*.

As mentioned in previous sections, minimal cycling of the pulse phases ensures that multiple coherence transfer pathways are collected simultaneously in the CPMG experiment. Aside from the first acquired echo, all subsequent echoes consist of a mixture of coherence transfer pathways. Thus, a well-defined echo train is obtained as shown in Fig. 4a. When pulse sequence delays are set incorrectly, the multiple pathways no longer form echoes at the same precise times, resulting in spectral distortion. For instance, when $\tau_1 \neq (\tau_a - p1)/2$, a time-domain 'splitting' of the echoes equal to $|\tau_a - p1 - 2\tau_1|$ is observed and the corresponding spikelet spectrum becomes modulated (Fig. 4b). The split echoes can be separated into two components (using a standard four-step phase cycle on p1): the coherence making up the first Hahn echo (denoted $p = -1$) and the symmetric coherence which is not observed during the first echo (denoted $p = +1$) as shown in Fig. 4c. The difference in position of the first echoes (relative to the start of the fid) for the two signals means that their resulting spectra will have different first-order phases. Indeed, it is not possible to have both spectra phased absorptively using a single set of phasing parameters. Therefore, in recording the two coherence transfer pathways simultaneously a destructive interference is caused by the convolution of spectra with differing first-order phases. An undistorted sum spectrum may be obtained if the two coherence transfer pathways are acquired and phased separately. However, a doubling of the total experimental time is required to obtain the same *S*/*N* as when both pathways are recorded simultaneously, i.e., a loss in efficiency by a factor of $\sqrt{2}$. Therefore, one should strive to collect both CPMG coherence transfer pathways simultaneously to maximize *S*/*N*. If for any reason this is not possible, separate acquisition of the two pathways would ensure that any artifacts caused by their destructive interference is avoided.

The preceding interpretation for the modulation of the spectral envelope lends insight into the spikelet representation of CPMG spectra. For illustration, the first four time-domain echoes from the ^{35}Cl NMR signal of Cp_2ZrCl_2 are shown separated in Fig. 5. As discussed above, the various echo timings yield spectra with different first-order phases. Addition of the individual spectra yields a spikelet spectrum. Baseline distortions between spikelets can be reduced with the inclusion of a greater number of echoes (not shown). Due to the τ_a periodicity of the time-domain echoes, spectral intensity is reinforced at intervals of $1/\tau_a$ from the transmitter frequency, while cancellation of intensity occurs elsewhere. Thus as is well known, spikelet spectra and powder patterns obtained from summation of the CPMG echoes are two representations of the same spectrum. In principle, the *S*/*N* enhancement observed for both representations is the same, while their integrated intensities will differ; further details can be found in Ref. [70].

2.4. Spikelet digitization

Distortion of the CPMG spikelet envelope may also arise during the fast Fourier transform (FFT) operation commonly used for NMR spectral processing. CPMG fids are often acquired using a combination of M cycles and points per τ_a which does not result in a total of 2^n data points (e.g., 256, 512 and 1024). However, FFT intrinsically requires 2^n data points. Hence, the number of data points in a fid may inadvertently be zero-filled to the next higher 2^n number upon FFT, leading to a modulation of the spectral envelope caused by disproportionate insertion of points into the sparsely digitized spikelets. For example, Fig. 6a and 6c shows two sets of spectra with a total of 16 echoes. The only difference between them is the number of points allotted per echo (100 and 128 for Fig. 6a and 6c, respectively), which add up to form fids with a total of 1600 and 2048 complex data points. Upon Fourier transformation,

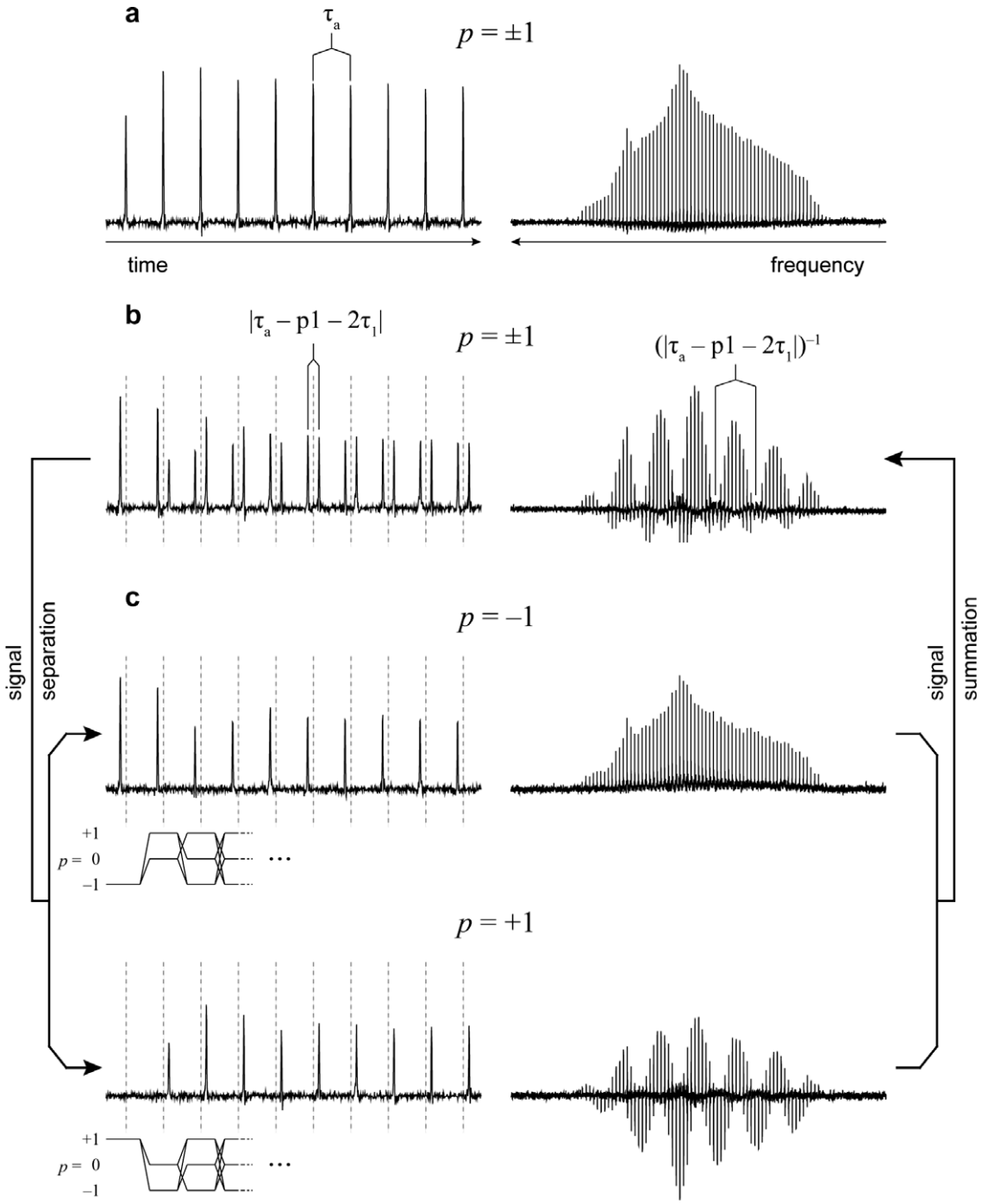

Fig. 4. ^{35}Cl NMR QCPMG time-domain signals and corresponding spectra of Cp_2ZrCl_2 at 19.6 T with (a) accurate and (b) inaccurate setting of τ_1. Vertical dashed lines in (b–c) denote the position of echoes in (a) which occur at times $(n + 1/2)\tau_a$. (b) When $\tau_1 \neq (\tau_a - p1)/2$, echoes are split by a time $|\tau_a - p1 - 2\tau_1|$ and the spikelet manifold is modulated by a frequency $(|\tau_a - p1 - 2\tau_1|)^{-1}$. Spectra were acquired using the pulse sequence in Fig. 1a with rf fields of 90.9 kHz, p1 = p2 = 1.3 μs, τ_1 = 50 μs, τ_2 = 20 μs, τ_a = 100 μs, M = 40, sw = 1.0 MHz and a recycle delay of 1.0 s. (c) Separation of the two components (denoted as $p = -1$ and + 1) making up the signal in (b) with their corresponding spectra processed using the same zero- and first-order phasing. The corresponding coherence transfer pathways are shown below fids.

the dataset with 2048 points displays the expected lines shape (Fig. 6c), but a distortion of the spikelet intensities is observed for the signal originally containing 1600 points because additional data points have been added to the dataset to comply with the FFT process (Fig. 6a). In this case, the spectrum is zero-filled to 2048 points automatically by the FFT operation. These extra points are incommensurate with the number of spikelets in the spectrum causing a modulation of the manifold. This effect is only apparent because there is a scarce number of points digitizing each spikelet. A number of zero-fills is necessary before the envelope modulation completely disappears as can be seen from the difference between the spectra zero-filled to 4096 points (remaining distortions are highlighted by the arrows). The dataset with 1600 points only starts to resemble the correct line shape upon zero-filling to 8192. These digitization artifacts are particularly severe if the echo train intensity has not fully decayed, which is the case for Fig. 6a. However, these distortions remain even when the signal has decayed, as shown in Fig. 6b where the time-domain signal has been

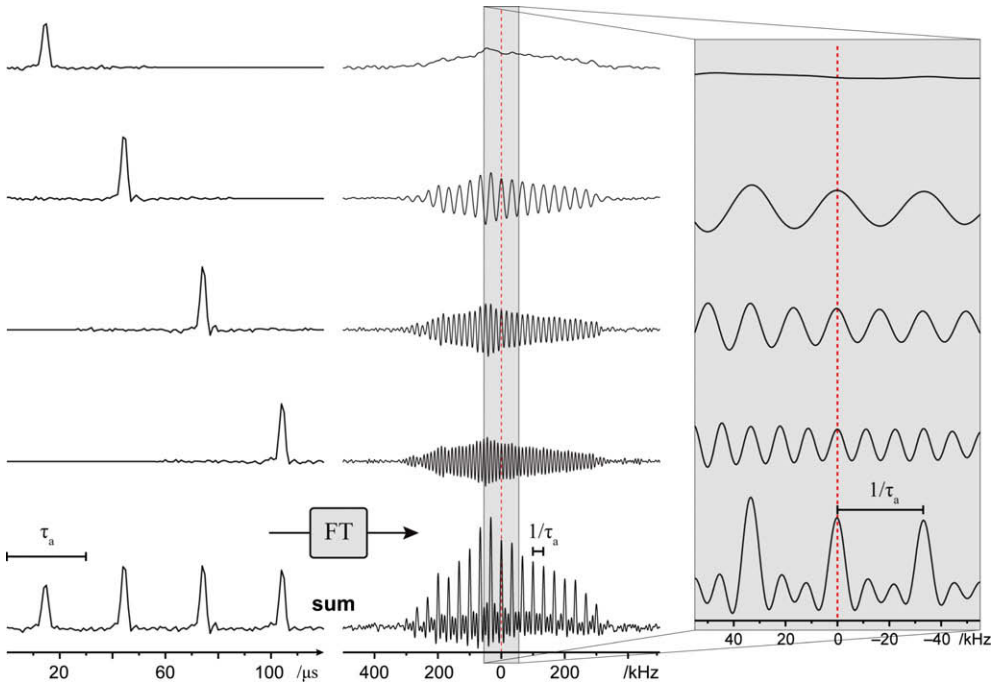

Fig. 5. Separation of the first four echoes in Fig. 4a illustrating the resemblance between (Q)CPMG spikelet spectra and typical powder patterns. Each echo contains the signal information for the complete powder pattern. However, the difference in time at which the echoes appear yield spectra with different first-order phases, which interfere destructively with each other except at the carrier frequency and at multiples of $1/\tau_a$. Expansion of the shaded area to the right shows the coherent superposition of signal intensity at the spikelet positions and destructive interference between spikelets. The echo spacing τ_a has been reduced to 30 μs for the sake of clarity when comparing the spectra with large first-order phase differences. Frequency scale is shown with respect to the transmitter position, which is denoted with a red dashed line. (For interpretation of color mentioned in this figure the reader is referred to the web version of the article.)

apodized prior to FFT; further apodization does not remove the distortions (not shown). In contrast, the correct line shape is always obtained from the dataset with a total of 2048 points regardless of zero-filling or the extent of truncation of the echo train, as shown in Fig. 6c and 6d. Therefore, acquisition of CPMG fids with a total 2^n data points is strongly recommended since the possibility for this kind of distortion is completely avoided. Alternatively, summation of the CPMG echoes prior to FFT would also produce spectra without distortions, since this digitization problem only occurs for the spikelet representation.

2.5. Refocusing flip angle

It is well known that short rf pulses are necessary for excitation of large bandwidths. This follows directly from the properties of Fourier spectroscopy, wherein the duration of events in the time-domain is inversely proportional to its corresponding spectral range in the frequency-domain. The CPMG refocusing pulse (p2) has traditionally been a 180°-pulse, which maximizes signal refocusing. However, many recent applications of CPMG have been for the examination of wideline spectra which tend to exceed the excitation bandwidth of standard monochromatic pulses, thus requiring acquisition of the complete spectrum in parts/segments [13,23,51]. In this context, the total experimental time will depend on: (1) the number of segments required to cover the complete powder pattern and (2) the time necessary to obtain adequate *S*/*N* for each individual segment. To this end, recent work using frequency-sweeps show considerable time savings compared to standard pulses [83,84]. Notably, a simple alternative for increasing the excitation bandwidth without modification of the pulse sequence can be achieved by reducing the p2 flip angle. Experiments and simulations (not shown) reveal that 180°-pulses only provide maximum intensity *at the transmitter frequency* and only a slight loss in intensity at the transmitter frequency is observed, accompanied by an increase in bandwidth, when p2 is shortened (Fig. 7). In particular, flip angles of 120–150° increase the breadth of the p2 excitation profile with minimal loss of intensity at the carrier frequency. Insensitivity to pulse flip angle is another one of the remarkable properties of CPMG which makes it applicable even in very inhomogeneous fields [94,95].

3. Excitation and refocusing using frequency sweeps

The recently reported WURST-QCPMG experiment [83] is based on a spin–echo sequence using frequency-swept chirp pulses [84], and has the same structure as the sequence shown in Fig. 1a except p1 and p2 are replaced by WURST-80 pulses [96] (Fig. 8a). Frequency sweeps provide a method of frequency-independent broadband excitation and refocusing which is not constrained by the *time* × *bandwidth* ≈ 1 relation of monochromatic pulses. Thus, their application to the acquisition of wideline spectra in combination with CPMG can greatly reduce experimental times [81]. The introduction of WURST pulses into the CPMG pulse sequence gives rise to a few peculiarities which merit consideration in addition to the practical considerations examined above for the CPMG experiment. Firstly, just as with the CPMG experiment, the τ_1 delay must be set accurately to account for the first WURST sweep duration, i.e., $\tau_1 = (\tau_a - p1)/2$. Otherwise, modulation of the spikelet envelope will arise as shown in Fig. 4. Due to the increased length of frequency-swept pulses compared to 'rectangular' pulses this condition is more stringent.

To the best of our knowledge, identical p1 and p2 pulses are always applied for the WURST-QCPMG experiment (i.e., both pulses have the same lengths p1 = p2, sweep rates $R_1 = R_2$ and rf fields $\nu_1(p1) = \nu_1(p2)$). The optimal rf field for broadband frequency-sweep excitation has previously been determined to be $\nu_1^{exc} \approx 0.26\sqrt{R_1}(I + 1/2)^{-1}$ [84,97,98], which is used for experimen-

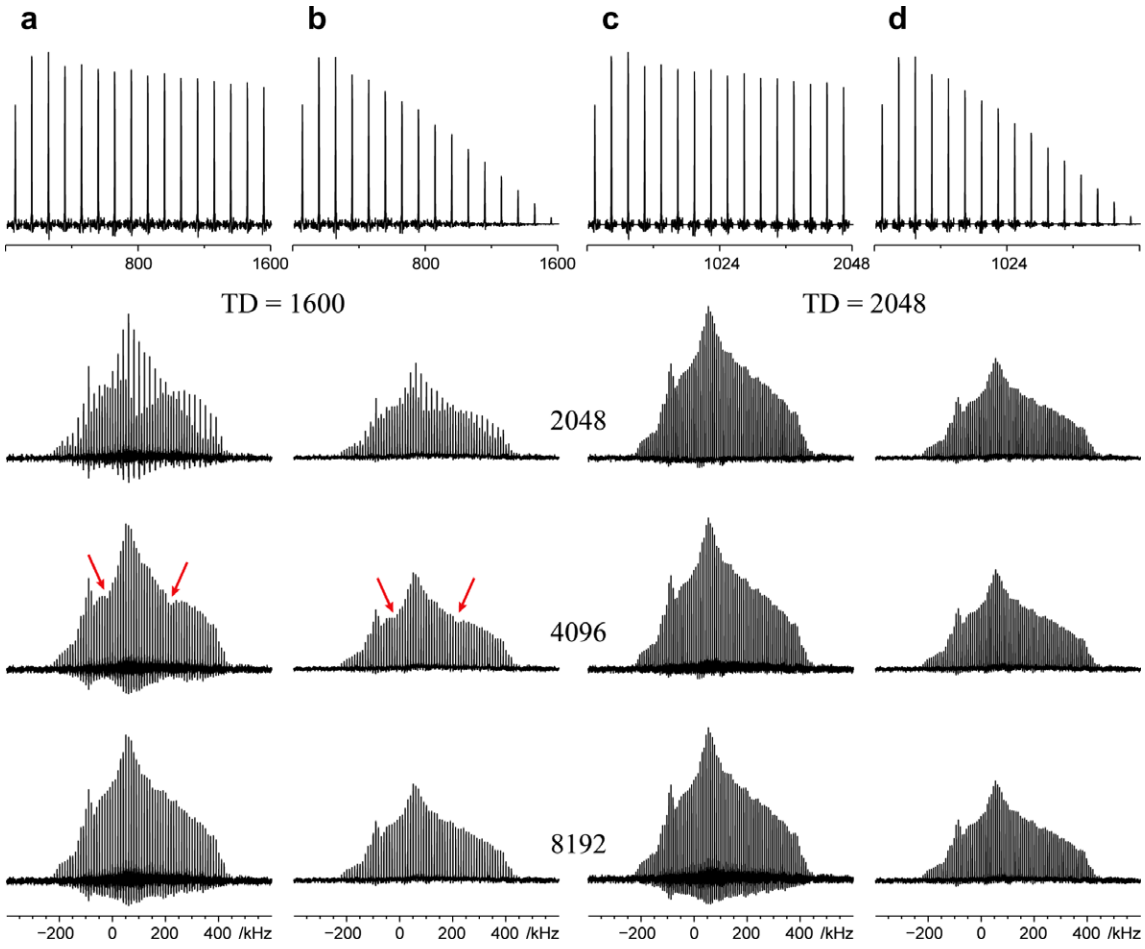

Fig. 6. Comparison of ^{35}Cl QCPMG spectra of Cp_2ZrCl_2 acquired at 19.6 T with a total of (a and b) 1600 and (c and d) 2048 complex data points zero-filled to 2048, 4096 and 8192 prior to FFT. The time-domain signals in columns (b) and (d) have been apodized using a sine function to reduce the effects of signal truncation. Arrows point to positions where distortions remain even after zero-filling. Modulation of the spikelet manifold arises due to the addition of points which are incommensurate with the number of poorly digitized spikelets.

tal optimization of the WURST-QCPMG sweep amplitudes [83]. Therefore, the typical WURST-QCPMG experiment can be considered analogous to a (90°–90°) quadrupolar-echo type of pulse sequence. The time-domain signal obtained using WURST-QCPMG exhibits a train of frequency-dispersed echoes, each of which resembles the frequency-domain powder pattern [84], instead of a train of sharp echoes usually observed when using hard pulses.

The frequency-dispersed time-domain echoes arise due to accumulation of second-order phase [84,99],

$$ph_2 = S \cdot \exp(i2\pi \sum_i \frac{\Delta p_i}{2R_i} f^2) \quad (2)$$

where R_i and Δp_i are the sweep rate and change in coherence level effected by pulse i, and f is the frequency variable ranging from $-sw/2$ to $+sw/2$. Fig. 8b shows the characteristic second-order phase modulation typically observed in WURST-QCPMG spectra, which is similar to the modulation observed when applying chirp pulses for broadband excitation [100]. For spin–echo experiments, the second-order phase can be compensated for by applying a refocusing pulse which has twice the sweep rate of the excitation pulse, $R_2 = 2R_1$ [84,97], in accordance with the equation for ph_2. However when $R_1 \neq R_2$ for WURST-QCPMG, a destructive interference results as shown in Fig. 8c due to the accumulation of different ph_2 by the $p = +1$ and -1 coherences. This is analogous to the difference in first-order phase observed for incorrect τ_1 settings (Fig. 4b). The second-order distortion may be avoided (with a $\sqrt{2}$ loss in efficiency) if the $p = \pm 1$ pathways are acquired with separate experiments and summed after proper processing, as with first-order distortions shown in Fig. 4. For the purpose of signal enhancement, R_1 and R_2 must be equal to obtain a coherent averaging of the $p = \pm 1$ pathways. A second-order phase correction can then be applied to obtain absorptively-phased spectra as shown in Fig. 8d.

Though R_1 and R_2 must be equal to maximize S/N, the same is not true for the p1 and p2 rf fields. To our knowledge, the rf field for maximum signal refocusing when $R_1 = R_2$ has not been reported in the literature. Experimentally, we have found that a maximum additional increase in the WURST-QCPMG signal of approximately 10% over most of the powder pattern can be obtained for the current sample when $\nu_1(\mathrm{p2}) \approx 2\nu_1(\mathrm{p1})$, as shown in Fig. 8e. Further increase in $\nu_1(\mathrm{p2})$ leads to signal loss due to phase dispersion, i.e., the second-order phase is no longer constant across the powder pattern. An intriguing consequence of employing these rf conditions is that φ_2 must be offset by approximately $\pi/2$ to observe the signal. Indeed, numerical simulations (not shown) also reveal that the 'effective' relative phase between p1 and p2 varies as a function of their rf field strengths. Further in-depth analysis of the relation between the phase and rf field strength of chirp pulses and the resulting NMR signal will be discussed elsewhere. A good strategy for obtaining the aforementioned signal increase is to offset φ_2 by $\pi/2$ and optimize $\nu_1(\mathrm{p2})$ around a starting point of approximately $2\nu_1(\mathrm{p1})$. If desired, the φ_2 offset and $\nu_1(\mathrm{p2})$ may then be optimized iteratively for maximum signal.

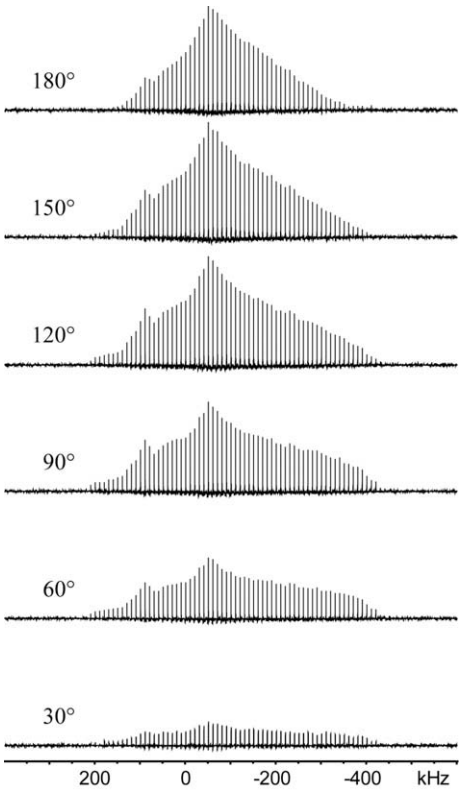

Fig. 7. ^{35}Cl QCPMG NMR spectra of Cp_2ZrCl_2 at 19.6 T varying the 'selective' flip angle of p2 using rf fields of 90.9 kHz and the pulse sequence in Fig. 1a with $\tau_1 = 50$ μs, $\tau_2 = 20$ μs, $\tau_a = 100$ μs, $M = 40$, $sw = 1.0$ MHz and a recycle delay of 1.0 s. Central-transition 'selective' pulses have durations reduced by the factor $(I + 1/2)$; for the case of ^{35}Cl ($I = 3/2$), conventional pulse widths are divided by 2.

4. Summary

The Carr–Purcell Meiboom–Gill pulse sequence is a very robust experiment which provides a straightforward method of signal enhancement for wideline NMR patterns of both spin-1/2 and quadrupolar nuclei. Herein we set forth guidelines for the practical implementation of the CPMG experiment:

1. The pulse sequence shown in Fig. 1a with a two-step phase cycle (following the guidelines in Section 2.1) is preferred for its simplicity and minimal chance of inaccurate parameter settings,
2. A p2 flip angle of 120–150° can be applied to maximize the excitation bandwidth,
3. The number of points per echo and CPMG cycles should result in 2^n total data points, and
4. Spectra should be absorptively-phased using a first-order phase correction of $\sim 360° \cdot \tau_a/(2\ \mathrm{dw})$.

CPMG acquisition using a two-step phase cycle may at times yield spectral modulation due to destructive interference between coherence transfer pathways. In such instances, application of a standard four-step phase cycle would ensure that these modulations are completely avoided at the expense of a $\sqrt{2}$ loss in S/N.

Frequency-swept pulses can be applied if excitation bandwidths greater than those achievable using monochromatic pulses are desired. For the WURST-QCPMG experiment:

1. The rates of the WURST pulses should be set so $R_1 = R_2$ to avoid spectral distortions,
2. In addition to zero- and first-order, spectra require second-order phase correction,
3. $\nu_1 \approx 0.26\sqrt{R_1}(I + 1/2)^{-1}$ can be used as a starting point for optimization of the WURST rf field strengths of both pulses, and,

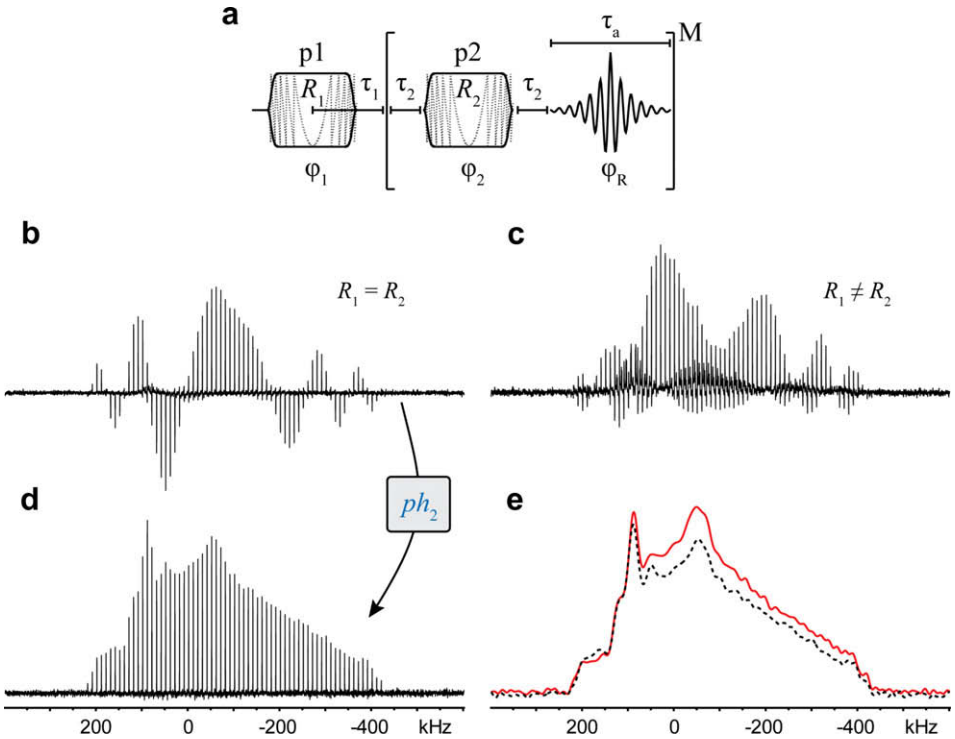

Fig. 8. (a) WURST-QCPMG pulse sequence. ^{35}Cl WURST-QCPMG spectra of Cp_2ZrCl_2 at 19.6 T using the parameters: (b,d) p1 = p2, $R_2 = R_1$ and $\nu_1(p2) = \nu_1(p1)$; (c) p1 = p2, $R_2 = 2R_1$ and $\nu_1(p2) = 2\nu_1(p1)$; (e) p1 = p2, $R_2 = R_1$ and $\nu_1(p2) = \nu_1(p1)$ (dashed black line) and p1 = p2, $R_2 = R_1$ and $\nu_1(p2) \approx 2\nu_1(p1)$ (solid red line), where R_i and $\nu_1(pi)$ are the sweep rates and rf fields for pulses i of length pi. Spectra in (b) and (c) were processed with and without second-order phasing, respectively. Spectra in (e) are obtained by summing of the QCPMG echoes, rather than Fourier transformation of the echo train, to facilitate visual comparison. Acquisition parameters: p1 = 50 μs, $R_1 = 20$ kHz·μs^{-1}, $\nu_1(p1) = 17.3$ kHz and WURST-80 [101]. (For interpretation of color mentioned in this figure the reader is referred to the web version of the article.)

4. The rf field strength of p2 can be further optimized around $\nu_1(p2) \approx 2\nu_1(p1)$ to obtain further gain in signal noting that the relative phase of the WURST pulses will vary as $\nu_1(p2)$ is increased.

Acknowledgments

This work was supported by the National High Magnetic Field Laboratory through National Science Foundation Cooperative Agreement (DMR-0084173). The reviewers are thanked for their helpful comments.

References

[1] M.E. Smith, E.R.H. van Eck, Recent advances in experimental solid state NMR methodology for half-integer spin quadrupolar nuclei, Prog. Nucl. Magn. Reson. Spectrosc. 34 (1999) 159–201.
[2] M.E. Smith, Recent progress in solid-state NMR of low-gamma nuclei, Ann. R. NMR S. 43 (2001) 121–175.
[3] S.E. Ashbrook, M.J. Duer, Structural information from quadrupolar nuclei in solid state NMR, Concept Magnetic Res. 28A (2006) 183–248.
[4] D. Massiot, I. Farnan, N. Gautier, D. Trumeau, A. Trokiner, J.P. Coutures, Ga-71 and Ga-69 nuclear-magnetic-resonance study of beta-Ga2O3 – resolution of 4-fold and 6-fold coordinated Ga sites in static conditions, Solid State Nucl. Magn. Reson. 4 (1995) 241–248.
[5] A. Medek, V. Frydman, L. Frydman, Central transition nuclear magnetic resonance in the presence of large quadrupole couplings: cobalt-59 nuclear magnetic resonance of cobaltophthalocyanines, J. Phys. Chem. A 103 (1999) 4830–4835.
[6] G. Wu, S. Dong, High-field I-127 NMR of solid sheelite structures: periodates revisited, Solid State Nucl. Magn. Reson. 20 (2001) 100–107.
[7] J.A. Tang, B.D. Ellis, T.H. Warren, J.V. Hanna, C.L.B. Macdonald, R.W. Schurko, Solid-state Cu-63 and Cu-65 NMR spectroscopy of inorganic and organometallic copper(I) complexes, J. Am. Chem. Soc. 129 (2007) 13049–13065.
[8] A.S. Lipton, R.W. Heck, G.R. Staeheli, M. Valiev, W.A. De Jong, P.D. Ellis, A QM/MM approach to interpreting Zn-67 solid-state NMR data in zinc proteins, J. Am. Chem. Soc. 130 (2008) 6224–6230.
[9] A.S. Lipton, R.W. Heck, S. Primak, D.R. McNeill, D.M. Wilson, P.D. Ellis, Characterization of Mg2+ binding to the DNA repair protein apurinic/apyrimidic endonuclease 1 via solid-state Mg-25 NMR spectroscopy, J. Am. Chem. Soc. 130 (2008) 9332–9341.
[10] Z.H. Gan, Measuring nitrogen quadrupolar coupling with C-13 detected wide-line N-14 NMR under magic-angle spinning, Chem. Commun. (2008) 868–870.
[11] M.A.M. Forgeron, R.E. Wasylishen, A solid-state Cr-53 NMR study of chromate and dichromate salts, Magn. Reson. Chem. 46 (2008) 206–214.
[12] F. Chen, G.B. Ma, R.G. Cavell, V.V. Terskikh, R.E. Wasylishen, Solid-state In-115 NMR study of indium coordination complexes, Chem. Commun. (2008) 5933–5935.
[13] A.J. Rossini, R.W. Mills, G.A. Briscoe, E.L. Norton, S.J. Geier, I. Hung, S. Zheng, J. Autschbach, R.W. Schurko, Solid-state chlorine NMR of group IV transition metal organometallic complexes, J. Am. Chem. Soc. 131 (2009) 3317–3330.
[14] F.H. Larsen, H.J. Jakobsen, P.D. Ellis, N.C. Nielsen, Sensitivity-enhanced quadrupolar-echo NMR of half-integer quadrupolar nuclei. Magnitudes and relative orientation of chemical shielding and quadrupolar coupling tensors, J. Phys. Chem. A 101 (1997) 8597–8606.
[15] H.Y. Carr, E.M. Purcell, Effects of diffusion on free precession in nuclear magnetic resonance experiments, Phys. Rev. 94 (1954) 630–638.
[16] S. Meiboom, D. Gill, Modified spin–echo method for measuring nuclear relaxation times, Rev. Sci. Instrum. 29 (1958) 688–691.
[17] R.L. Vold, G.L. Hoatson, L. Vugmeyster, D. Ostrovsky, P.J. De Castro, Solid state deuteron relaxation time anisotropy measured with multiple-echo acquisition, Phys. Chem. Chem. Phys. 11 (2009) 7008–7012.
[18] L.A. O'Dell, R.W. Schurko, Fast and simple acquisition of solid-state 14N NMR spectra with signal enhancement via population transfer, J. Am. Chem. Soc. 131 (2009) 6658–6659.
[19] L.A. O'Dell, R.W. Schurko, Static solid-state 14N NMR and computational studies of nitrogen EFG tensors in some crystalline amino acids, Phys. Chem. Chem. Phys. 11 (2009) 7069–7077.
[20] F.H. Larsen, S. Rossano, I. Farnan, Order and disorder in titanosilicate glass by O-17 MAS off-MAS and 3Q-QCPMG-MAS solid-state NMR, J. Phys. Chem. B 111 (2007) 8014–8019.
[21] F.H. Larsen, I. Farnan, Si-29 and O-17 (Q)CPMG-MAS solid-state NMR experiments as an optimum approach for half-integer nuclei having long T-1 relaxation times, Chem. Phys. Lett. 357 (2002) 403–408.
[22] I. Hung, R.W. Schurko, Solid-state Mg-25 QCPMG NMR of bis(cyclopentadienyl)magnesium, Solid State Nucl. Magn. Reson. 24 (2003) 78–93.
[23] J.F. Zhu, Z. Lin, Z.M. Yan, Y.N. Huang, Zr-91 and Mg-25 solid-state NMR characterization of the local environments of the metal centers in microporous materials, Chem. Phys. Lett. 461 (2008) 260–265.
[24] F.H. Larsen, J. Skibsted, H.J. Jakobsen, N.C. Nielsen, Solid-state QCPMG NMR of low-gamma quadrupolar metal nuclei in natural abundance, J. Am. Chem. Soc. 122 (2000) 7080–7086.
[25] M.C. Davis, W.J. Brouwer, D.J. Wesolowski, L.M. Anovitz, A.S. Lipton, K.T. Mueller, Magnesium silicate dissolution investigated by 29Si MAS, 1H-29Si CPMAS, 25Mg QCPMG, and 1H-25Mg CP QCPMG NMR, Phys. Chem. Chem. Phys. 11 (2009) 7013–7021.
[26] F.H. Larsen, I. Farnan, Site populations and short range order in aluminosilicates investigated by Al-27 solid-state NMR, J. Phys. Chem. B 108 (2004) 9764–9771.
[27] R. Lefort, J.W. Wiench, M. Pruski, J.P. Amoureux, Optimization of data acquisition and processing in Carr–Purcell–Meiboom–Gill multiple-quantum magic angle spinning nuclear magnetic resonance, J. Chem. Phys. 116 (2002) 2493–2501.
[28] J.A. Tang, J.D. Masuda, T.J. Boyle, R.W. Schurko, Ultra-wideline Al-27 NMR investigation of three- and five-coordinate aluminum environments, ChemPhysChem 7 (2006) 117–130.
[29] L.A. O'Dell, K. Klimm, J.C.C. Freitas, S.C. Kohn, M.E. Smith, S-33 MAS NMR of a disordered sulfur-doped silicate: signal enhancement via RAPT, QCPMG and adiabatic pulses, Appl. Magn. Reson. 35 (2008) 247–259.
[30] D.L. Bryce, M. Gee, R.E. Wasylishen, High-field chlorine NMR spectroscopy of solid organic hydrochloride salts: a sensitive probe of hydrogen bonding environment, J. Phys. Chem. A 105 (2001) 10413–10421.
[31] D.L. Bryce, G.D. Sward, Chlorine-35/37 NMR spectroscopy of solid amino acid hydrochlorides: refinement of hydrogen-bonded proton positions using experiment and theory, J. Phys. Chem. B 110 (2006) 26461–26470.
[32] D.L. Bryce, E.B. Bultz, Alkaline earth chloride hydrates: chlorine quadrupolar and chemical shift tensors by solid-state NMR spectroscopy and plane wave pseudopotential calculations, Chem.-Eur. J. 13 (2007) 4786–4796.
[33] C.M. Widdifield, R.W. Schurko, A solid-state K-39 and C-13 NMR study of polymeric potassium metallocenes, J. Phys. Chem. A 109 (2005) 6865–6876.
[34] R.W. Schurko, I. Hung, C.M. Widdifield, Signal enhancement in NMR spectra of half-integer quadrupolar nuclei via DFS-QCPMG and RAPT-QCPMG pulse sequences, Chem. Phys. Lett. 379 (2003) 1–10.
[35] F.H. Larsen, I. Farnan, A.S. Lipton, Separation of Ti-47 and Ti-49 solid-state NMR lineshapes by static QCPMG experiments at multiple fields, J. Magn. Reson. 178 (2006) 228–236.
[36] D. Padro, V. Jennings, M.E. Smith, R. Hoppe, P.A. Thomas, R. Dupree, Variations of titanium interactions in solid state NMR-correlations to local structure, J. Phys. Chem. B 106 (2002) 13176–13185.
[37] J. Zhu, N. Trefiak, T.K. Woo, Y. Huang, A 47/49Ti solid-state NMR study of layered titanium phosphates at ultrahigh magnetic field, J. Phys. Chem. C 113 (2009) 10029–10037.
[38] K.J. Ooms, K.W. Feindel, V.V. Terskikh, R.E. Wasylishen, Ultrahigh-field NMR spectroscopy of quadrupolar transition metals: Mn-55 NMR of several solid manganese carbonyls, Inorg. Chem. 45 (2006) 8492–8499.
[39] P. Crewdson, D.L. Bryce, F. Rominger, P. Hofmann, Application of ultrahigh-field Co-59 solid-state NMR spectroscopy in the investigation of the 1,2-polybutadiene catalyst Co(C8H13)(C4H6), Angew. Chem.-Int. Edit. 47 (2008) 3454–3457.
[40] F.H. Larsen, A.S. Lipton, H.J. Jakobsen, N.C. Nielsen, P.D. Ellis, Zn-67 QCPMG solid-state NMR studies of zinc complexes as models for metalloproteins, J. Am. Chem. Soc. 121 (1999) 3783–3784.
[41] A.S. Lipton, G.W. Buchko, J.A. Sears, M.A. Kennedy, P.D. Ellis, Zn-67 solid-state NMR spectroscopy of the minimal DNA binding domain of human nucleotide excision repair protein XPA, J. Am. Chem. Soc. 123 (2001) 992–993.
[42] A.S. Lipton, C. Bergquist, G. Parkin, P.D. Ellis, Solid-state Zn-67 NMR spectroscopic studies and ab initio molecular orbital calculations on a synthetic analogue of carbonic anhydrase, J. Am. Chem. Soc. 125 (2003) 3768–3772.
[43] A.S. Lipton, R.W. Heck, P.D. Ellis, Zinc solid-state NMR spectroscopy of human carbonic anhydrase: Implications for the enzymatic mechanism, J. Am. Chem. Soc. 126 (2004) 4735–4739.
[44] A.S. Lipton, R.W. Heck, J.A. Sears, P.D. Ellis, Low temperature solid-state NMR experiments of half-integer quadrupolar nuclides: caveats and data analysis, J. Magn. Reson. 168 (2004) 66–74.
[45] A.S. Lipton, P.D. Ellis, Modeling the metal center of Cys(4) zinc proteins, J. Am. Chem. Soc. 129 (2007) 9192–9200.
[46] A.S. Lipton, R.W. Heck, M. Hernick, C.A. Fierke, P.D. Ellis, Residue ionization in LpxC directly observed by Zn-67 NMR spectroscopy, J. Am. Chem. Soc. 130 (2008) 12671–12679.
[47] A.S. Lipton, M.M. Morlok, G. Parkin, P.D. Ellis, Zn-67 solid-state NMR spectroscopy of {Tp(But, Me) Zn(OH2)} HOB(C6F5)(3). The importance of the anion HOB(C6F5)(3) (-), Inorg. Chem. 47 (2008) 5184–5189.
[48] J.T. Cheng, P.D. Ellis, Adsorption of Rb+ to gamma-alumina as followed by solid-state Rb-87 NMR-spectroscopy, J. Phys. Chem. 93 (1989) 2549–2555.
[49] I. Hung, R.W. Schurko, Solid-state Zr-91 NMR of bis(cyclopentadienyl)dichlorozirconium(IV), J. Phys. Chem. B 108 (2004) 9060–9069.
[50] A.Y.H. Lo, T.E. Bitterwolf, C.L.B. Macdonald, R.W. Schurko, Solid-state Nb-93 and C-13 NMR investigations of half-sandwich niobium(I) and niobium(V) cyclopentadienyl complexes, J. Phys. Chem. A 109 (2005) 7073–7087.

[51] M.A.M. Forgeron, R.E. Wasylishen, Molybdenum magnetic shielding and quadrupolar tensors for a series of molybdate salts: a solid-state Mo-95 NMR study, Phys. Chem. Chem. Phys. 10 (2008) 574–581.
[52] M.A.M. Forgeron, R.E. Wasylishen, A solid-state Mo-95 NMR and computational investigation of dodecahedral and square antiprismatic octacyanomolybdate(IV) anions: is the point-charge approximation an accurate probe of local symmetry?, J Am. Chem. Soc. 128 (2006) 7817–7827.
[53] A. Sutrisno, C. Lu, R.H. Lipson, Y. Huang, Combined 135/137Ba solid-state NMR at an ultrahigh magnetic field and computational study of beta-barium borate, J. Phys. Chem. C (2009) ACS ASAP.
[54] H. Hamaed, M.W. Laschuk, V.V. Terskikh, R.W. Schurko, Application of solid-state 209Bi NMR to the structural characterization of bismuth-containing materials, J. Am. Chem. Soc. 131 (2009) 8271–8279.
[55] R. Siegel, T.T. Nakashima, R.E. Wasylishen, Signal-to-noise enhancement of NMR spectra of solids using multiple-pulse spin–echo experiments, Concept Magnetic Res. 26A (2005) 62–77.
[56] R. Siegel, T.T. Nakashima, R.E. Wasylishen, Application of multiple-pulse experiments to characterize broad NMR chemical-shift powder patterns from spin-1/2 nuclei in the solid state, J. Phys. Chem. B 108 (2004) 2218–2226.
[57] I. Hung, A.J. Rossini, R.W. Schurko, Application of the Carr–Purcell Meiboom–Gill pulse sequence for the acquisition of solid-state NMR spectra of spin-(1)/(2) nuclei, J. Phys. Chem. A 108 (2004) 7112–7120.
[58] S.E. Shore, J.P. Ansermet, C.P. Slichter, J.H. Sinfelt, NMR-study of the bonding and diffusion of Co chemisorbed on Pd, Phys. Rev. Lett. 58 (1987) 953–956.
[59] S.M. Desoto, C.P. Slichter, A.M. Kini, H.H. Wang, U. Geiser, J.M. Williams, C-13 NMR-studies of the normal and superconducting states of the organic superconductor kappa-(Et)(2)Cu N(CN)(2) Br, Phys. Rev. B 52 (1995) 10364–10368.
[60] S.E. Barrett, D.J. Durand, C.H. Pennington, C.P. Slichter, T.A. Friedmann, J.P. Rice, D.M. Ginsberg, Cu-63 knight-shifts in the superconducting state of YBa2Cu3O7-delta(T_c=90 K), Phys. Rev. B 41 (1990) 6283–6296.
[61] J.A. Tang, E. Kogut, D. Norton, A.J. Lough, B.R. McGarvey, U. Fekl, R.W. Schurko, Impact of reduction on the properties of metal bisdithiolenes: multinuclear solid-state NMR and structural studies on Pt(tfd)2 and its reduced forms, J. Phys. Chem. B 113 (2009) 3298–3313.
[62] J.W. Wiench, V.S.Y. Lin, M. Pruski, Si-29 NMR in solid state with CPMG acquisition under MAS, J. Magn. Reson. 193 (2008) 233–242.
[63] J. Trebosc, J.W. Wiench, S. Huh, V.S.Y. Lin, M. Pruski, Studies of organically functionalized mesoporous silicas using heteronuclear solid-state correlation NMR spectroscopy under fast magic angle spinning, J. Am. Chem. Soc. 127 (2005) 7587–7593.
[64] I. Farnan, H. Cho, W.J. Weber, R.D. Scheele, N.R. Johnson, A.E. Kozelisky, High-resolution solid-state nuclear magnetic resonance experiments on highly radioactive ceramics, Rev. Sci. Instrum. 75 (2004) 5232–5236.
[65] B.A. Cowans, J.B. Grutzner, Examination of homogeneous broadening in solids via rotationally synchronized spin–echo NMR-spectroscopy, J. Magn. Reson. A 105 (1993) 10–18.
[66] A. Pines, W. Rhim, J.S. Waugh, Homogeneous and Inhomogeneous nuclear spin echoes in solids, J. Magn. Reson. 6 (1972) 457–@@-.
[67] A.N. Garroway, Homogeneous and inhomogeneous nuclear-spin echoes in organic solids – adamantane, J. Magn. Reson. 28 (1977) 365–371.
[68] F.H. Larsen, H.J. Jakobsen, P.D. Ellis, N.C. Nielsen, QCPMG-MAS NMR of half-integer quadrupolar nuclei, J. Magn. Reson. 131 (1998) 144–147.
[69] F.H. Larsen, H.J. Jakobsen, P.D. Ellis, N.C. Nielsen, High-field QCPMG-MAS NMR of half-integer quadrupolar nuclei with large quadrupole couplings, Mol. Phys. 95 (1998) 1185–1195.
[70] J.Z. Hu, R.A. Wind, Sensitivity-enhanced phase-corrected ultra-slow magic angle turning using multiple-echo data acquisition, J. Magn. Reson. 163 (2003) 149–162.
[71] K.H. Lim, T. Nguyen, T. Mazur, D.E. Wemmer, A. Pines, Sensitivity enhancement in multiple-quantum NMR experiments with CPMG detection, J. Magn. Reson. 157 (2002) 160–162.
[72] G. Mali, V. Kaucic, Enhancing sensitivity or resolution of homonuclear correlation experiment for half-integer quadrupolar nuclei, J. Magn. Reson. 171 (2004) 48–56.
[73] T. Vosegaard, F.H. Larsen, H.J. Jakobsen, P.D. Ellis, N.C. Nielsen, Sensitivity-enhanced multiple-quantum MAS NMR of half-integer quadrupolar nuclei, J. Am. Chem. Soc. 119 (1997) 9055–9056.
[74] F.H. Larsen, N.C. Nielsen, Effects of finite rf pulses and sample spinning speed in multiple-quantum magic-angle spinning (MQ-MAS) and multiple-quantum quadrupolar Carr–Purcell–Meiboom–Gill magic-angle spinning (MQ-QCPMG-MAS) nuclear magnetic resonance of half-integer quadrupolar nuclei, J. Phys. Chem. A 103 (1999) 10825–10832.
[75] I. Hung, K. Shetty, P.D. Ellis, W.W. Brey, Z.H. Gan, High-field QCPMG NMR of large quadrupolar patterns using resistive magnets, Solid State Nucl. Magn. Reson. 36 (2009) 159–163.
[76] M.A. Kennedy, R.L. Vold, R.R. Vold, Stepped-frequency NMR-spectroscopy, J. Magn. Reson. 92 (1991) 320–331.
[77] T.J. Bastow, M.E. Smith, S.N. Stuart, Observation of Zr-91 NMR in zirconium-based metals and oxides, Chem. Phys. Lett. 191 (1992) 125–129.
[78] A.S. Lipton, T.A. Wright, M.K. Bowman, D.L. Reger, P.D. Ellis, Solid-state Zn-67 NMR spectroscopy in bioinorganic chemistry. Spectra of four- and six-coordinate zinc pyrazolylborate complexes obtained by management of proton relaxation rates with a paramagnetic dopant, J. Am. Chem. Soc. 124 (2002) 5850–5860.
[79] K. Yamauchi, J.W.G. Janssen, A.P.M. Kentgens, Implementing solenoid microcoils for wide-line solid-state NMR, J. Magn. Reson. 167 (2004) 87–96.
[80] D. Sakellariou, G. Le Goff, J.F. Jacquinot, High-resolution, high-sensitivity NMR of nanolitre anisotropic samples by coil spinning, Nature 447 (2007) 694.
[81] J.A. Tang, L.A. O'Dell, P.M. Aguiar, B.E.G. Lucier, D. Sakellariou, R.W. Schurko, Application of static microcoils and WURST pulses for solid-state ultra-wideline NMR spectroscopy of quadrupolar nuclei, Chem. Phys. Lett. 466 (2008) 227–234.
[82] L.A. O'Dell, A.J. Rossini, R.W. Schurko, Acquisition of ultra-wideline NMR spectra from quadrupolar nuclei by frequency stepped WURST-QCPMG, Chem. Phys. Lett. 468 (2009) 330–335.
[83] L.A. O'Dell, R.W. Schurko, QCPMG using adiabatic pulses for faster acquisition of ultra-wideline NMR spectra, Chem. Phys. Lett. 464 (2008) 97–102.
[84] R. Bhattacharyya, L. Frydman, Quadrupolar nuclear magnetic resonance spectroscopy in solids using frequency-swept echoing pulses, J. Chem. Phys. 127 (2007) 194503.
[85] A.S. Lipton, J.A. Sears, P.D. Ellis, A general strategy for the NMR observation of half-integer quadrupolar nuclei in dilute environments, J. Magn. Reson. 151 (2001) 48–59.
[86] F.H. Larsen, H.J. Jakobsen, P.D. Ellis, N.C. Nielsen, Molecular dynamics from H-2 quadrupolar Carr–Purcell–Meiboom–Gill solid-state NMR spectroscopy, Chem. Phys. Lett. 292 (1998) 467–473.
[87] F.H. Larsen, Molecular dynamics of half-integer quadrupolar nuclei studied by QCPMG solid-state NMR experiments on static and rotating samples theory and simulations, J. Magn. Reson. 171 (2004) 293–304.
[88] G. Goelman, M.G. Prammer, The CPMG pulse sequence in strong magnetic-field gradients with applications to oil-well logging, J. Magn. Reson. A 113 (1995) 11–18.
[89] T. Nagele, U. Klose, W. Grodd, Numerically optimized Rf-refocusing pulses in localized MR proton spectroscopy, Magn. Reson. Imag. 11 (1993) 785–797.
[90] P. Leroux, R.S. Hinks, Stabilization of echo amplitudes in FSE sequences, Magn. Reson. Med. 30 (1993) 183–190.
[91] E.L. Hahn, Spin echoes, Phys. Rev. 80 (1950) 580–594.
[92] M. Bak, J.T. Rasmussen, N.C. Nielsen, SIMPSON: a general simulation program for solid-state NMR spectroscopy, J. Magn. Reson. 147 (2000) 296–330.
[93] F. Balibanu, K. Hailu, R. Eymael, D.E. Demco, B. Blumich, Nuclear magnetic resonance in inhomogeneous magnetic fields, J. Magn. Reson. 145 (2000) 246–258.
[94] M.D. Hurlimann, Encoding of diffusion and T-1 in the CPMG echo shape: Single-shot D and T-1 measurements in grossly inhomogeneous fields, J. Magn. Reson. 184 (2007) 114–129.
[95] R.I. Chelcea, R. Fechete, E. Culea, D.E. Demco, B. Blumich, Distributions of transverse relaxation times for soft-solids measured in strongly inhomogeneous magnetic fields, J. Magn. Reson. 196 (2009) 178–190.
[96] E. Kupce, R. Freeman, Adiabatic pulses for wide-band inversion and broad-band decoupling, J. Magn. Reson. A 115 (1995) 273–276.
[97] J.M. Bohlen, M. Rey, G. Bodenhausen, Refocusing with chirped pulses for broad-band excitation without phase dispersion, J. Magn. Reson. 84 (1989) 191–197.
[98] Y. Shrot, L. Frydman, Spatially encoded NMR and the acquisition of 2D magnetic resonance images within a single scan, J. Magn. Reson. 172 (2005) 179–190.
[99] I. Hung, Z.H. Gan, J. Magn. Reson. (2010), in preparation.
[100] J.M. Bohlen, G. Bodenhausen, Experimental aspects of chirp NMR-spectroscopy, J. Magn. Reson. A 102 (1993) 293–301.
[101] E. Kupce, R. Freeman, Stretched adiabatic pulses for broadband spin inversion, J. Magn. Reson. A 117 (1995) 246–256.